

Development of a Universal Correction Algorithm for Filter-Based Absorption Photometers

Hanyang Li¹, Gavin R. McMeeking², and Andrew A. May¹

1 The Ohio State University Department of Civil, Environmental, and Geodetic Engineering, Columbus, Ohio, USA

2 Handix Scientific, LLC, Boulder, Colorado, USA

Corresponding author: Andrew A. May (may.561@osu.edu).

This Word document includes:

- Supplementary Text (Pages 2-7)
 1. Developing the model described in Section 2.3.3
 - Prediction of $\frac{B_{abs}}{B_{ATN}}$ using multiple regression models
 - Transformation of the regression models
 - Assessment of the fit of regression models
 - Interpretation of the regression models
 2. The procedure for simulating the uncertainty of the new algorithms in Section 3.5
- Tables S5 to S12 (Pages 8-13)
 - **S5.** Relationship between the corrected filter-based B_{abs} (FIREX-TAP and SGP-PSAP) and the reference B_{abs} .
 - **S6.** Inter-comparison between different filter-based B_{abs} corrected by the same algorithm.
 - **S7-S11.** Updated coefficients in the B1999 and V2005 algorithms using our data.
 - **S12.** The quartile deviation of the derived coefficient values in our algorithm.
- Figures S5 to S13 (Pages 14-19)
 - **S5.** Relationship between the corrected filter-based B_{abs} (FIREX-TAP and SGP-PSAP) and the reference B_{abs} .
 - **S6.** Relationship between the corrected FIREX-AETH and the reference B_{abs} .
 - **S7.** The distribution of derived coefficient values in our algorithm.
 - **S8.** Inter-comparison between the SGP-CLAP B_{abs} corrected by “Algorithm C” and reference B_{abs} .
 - **S9-S10.** The distribution of SSA calculated by different combinations of B_{abs} and B_{scat} .
 - **S11.** The distribution of AAE and SSA computed by the new algorithms (A, B, C)
 - **S12.** The distribution of AAE calculated by different wavelength combinations.
 - **S13.** Inter-comparison of SGP-CLAP B_{abs} derived by the new algorithm with different calculation of AAE.
- References (Page 20)

SUPPLEMENTARY TEXT

1. Developing the model described in Section 2.3.3

Statistical regression analyses were performed to predict $\frac{B_{abs}}{B_{ATN}}$ (dependent variable) in Eq. (9). The analyses were applied on a total of 2676 FIREX observations (PAX-derived B_{abs} , CLAP-derived B_{ATN} , Tr, SSA, and AAE) at three wavelengths (467 nm, 528 nm, and 652 nm). Table S1 summarizes the variables used in the analyses. The statistical software R was used for all analyses.

Table S1 Descriptive statistics for the variables under consideration as inputs to the correction algorithm.

	B_{abs}			B_{ATN}			$B_{abs} \setminus B_{ATN}$			Tr			SSA			AAE
	467 nm	528 nm	652 nm	467 nm	528 nm	652 nm	467 nm	528 nm	652 nm	467 nm	528 nm	652 nm	467 nm	528 nm	652 nm	
Min.	45.0	38.5	29.5	162.0	140.1	98.9	0.14	0.12	0.10	0.27	0.34	0.45	0.27	0.25	0.21	1.25
1st Qu.	125.4	99.9	64.8	473.7	413.3	296.5	0.22	0.20	0.18	0.55	0.60	0.70	0.50	0.47	0.44	1.52
Median	216.5	169.5	112.1	843.9	721.8	528.5	0.25	0.23	0.21	0.66	0.71	0.79	0.72	0.72	0.70	1.72
Mean	320.2	245.9	160.2	1276.7	1091.0	781.6	0.26	0.24	0.22	0.68	0.72	0.79	0.66	0.66	0.65	1.99
3rd Qu.	407.5	316.2	203.7	1658.2	1418.6	1000.9	0.30	0.27	0.25	0.80	0.83	0.88	0.84	0.84	0.84	2.34
Max.	2370.9	1689.2	1295.8	11227.0	9280.7	6391.2	0.45	0.43	0.40	1.00	1.00	1.00	0.95	0.96	0.97	4.07

Figure S1 shows the relationships between $\frac{B_{abs}}{B_{ATN}}$ and each independent variable. It is clear that $\frac{B_{abs}}{B_{ATN}}$ increases with decreasing Tr, SSA, and AAE. However, the relationships are nonlinear, and the data points scatter fairly widely. Moreover, $\frac{B_{abs}}{B_{ATN}}$ spans a wide range of values at a single value of Tr, which inspired us to investigate the interactions among Tr, SSA, and AAE.

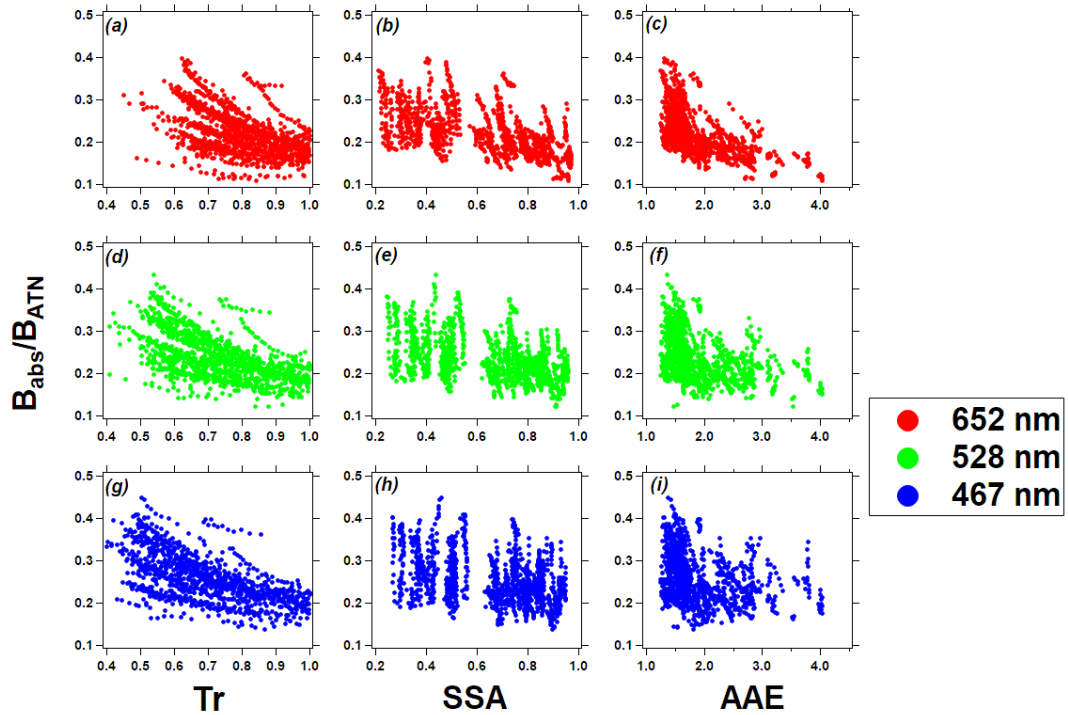


Figure S1. Scatter plot of $\frac{B_{abs}}{B_{ATN}}$ against Tr, SSA, and AAE at 652 nm, 528 nm, and 467 nm.

- Prediction of $\frac{B_{abs}}{B_{ATN}}$ using multiple regression models

Independent variables of $\frac{B_{abs}}{B_{ATN}}$ were identified by “best subset regression” (using both adjusted R^2 and Mallows’ C_p as the criterion) and “stepwise regression” (both forward and backward). Variables tested for significance included Tr, SSA, AAE, and three-way interactions (Tr: SSA, Tr: AAE, SSA: AAE, and Tr: SSA: AAE). Regardless of wavelength, the best-subset models selected the same form of regression, which included all independent variables and the intercept (Table S2). However, the stepwise regression models varied across wavelengths: at 652 nm, the forward stepwise model was same as the best-subset models, but the backward stepwise model dropped two variables (Tr: AAE and Tr: SSA: AAE); at 528 nm and 467 nm, forward and backward stepwise regression produced the same model at each wavelength, but the selected variables were different at different wavelengths (see Table S2). Generally, the adjusted R^2 of best-subset models was greater or equal to the adjusted R^2 of stepwise models at each wavelength. As we placed a higher priority on prediction accuracy of $\frac{B_{abs}}{B_{ATN}}$, we selected the models that result in the greatest adjusted R^2 (the model including seven predictors).

Table S2 Predictors of $\frac{B_{abs}}{B_{ATN}}$ using “best subset regression” and “stepwise regression”.

	652 nm			528 nm		467 nm	
	Best subset	Stepwise (forward)	Stepwise (backward)	Best subset	Stepwise ^a	Best subset	Stepwise ^a
R^2	0.620	0.620	0.607	0.544	0.510	0.531	0.531
Intercept	1.08±0.15	1.08±0.15	0.84±0.03	1.21±0.15	0.84±0.03	1.39±0.16	1.39±0.16
	***	***	***	***	***	***	***
Tr	-0.75±0.19	-0.75±0.19	-0.45±0.03	-0.89±0.20	-0.37±0.03	-1.12±0.23	-1.12±0.23
	***	***	***	***	***	***	***
SSA	-0.86±0.15	-0.86±0.15	-0.53±0.04	-0.89±0.15	-0.46±0.04	-1.07±0.17	-1.07±0.17
	***	***	***	***	***	***	***
AAE	-0.30±0.10	-0.30±0.10	-0.15±0.02	-0.44±0.10	-0.20±0.02	-0.57±0.11	-0.57±0.11
	**	**	***	***	***	***	***
Tr: SSA	0.79±0.19	0.79±0.19	0.38±0.04	0.77±0.21	0.17±0.04	0.99±0.25	0.99±0.25
	***	***	***	***	***	***	***
SSA: AAE	0.31±0.11	0.31±0.11	0.13±0.02	0.47±0.11	0.20±0.02	0.64±0.12	0.64±0.12
	**	**	***	***	***	***	***
Tr: AAE	0.19±0.13	0.19±0.13		0.34±0.14		0.51±0.16	0.51±0.16
	.	.		*		**	**
Tr: SSA: AAE	-0.24±0.13	-0.24±0.13		-0.38±0.14		-0.59±0.17	-0.59±0.17
	.	.		**		***	***
*** p < 0.001; ** p < 0.01; * p < 0.05; . p < 0.1.							

^a At 528 nm and 467 nm, forward and backward stepwise approaches output the same regression model.

- *Transformation of the regression models*

A nonlinear transformation of variables is commonly used if a non-linear relationship exists between the independent and dependent variables (e.g., (Benoit, 2011; Creamer et al., 1989; Lek et al., 1996)). As seen in the first column in Fig. S1, there appears to be a logarithmic relationship between $\frac{B_{abs}}{B_{ATN}}$ and Tr, implying that logarithmic transformation of the regression model likely improve the performance of the regression model. We tried nonlinear transformation of the dependent variable. The results generally did not improve the regression results (the adjusted R^2 is smaller or equal to that of the original model); therefore, the original $\frac{B_{abs}}{B_{ATN}}$ was retained. Then, we transformed the dependent variables. Using $\ln(Tr)$ instead of Tr in the models improved the adjusted R^2 from 0.54 to 0.57 (528 nm) and from 0.53 to 0.58 (467 nm), but no improvement at 652 nm. Moreover, $\ln(Tr)$ has a physical meaning in that $\ln(Tr) = -ATN$, so the transformed results are easy to interpret. Consequently, we adopted $\ln(Tr)$ in the regression model. No improvement was found using the transformation of SSA and AAE; therefore, the original SSA and AAE were retained. We present the results of the regression models using logarithmic transformation of Tr in Table S3.

Table S3 Predictors of $\frac{B_{abs}}{B_{ATN}}$ (similar to Table S2, but using $\ln(Tr)$ instead of Tr in the model)

	652 nm	528 nm	467 nm
R^2	0.62	0.57	0.58
Intercept	0.36±0.04	0.34±0.06	0.30±0.07
	***	***	***
$\ln(Tr)$	-0.61±0.15	-0.73±0.14	-0.87±0.15
	***	***	***
SSA	-0.09±0.04	-0.14±0.06	-0.11±0.07
	*	*	.
AAE	-0.12±0.03	-0.11±0.04	-0.06±0.05
	***	**	.
$\ln(Tr)$: SSA	0.61±0.15	0.60±0.14	0.73±0.16
	***	***	***
SSA: AAE	0.09±0.03	0.09±0.04	0.06±0.03
	**	*	.
$\ln(Tr)$: AAE	0.19±0.10	0.33±0.10	0.45±0.10
	.	***	***
$\ln(Tr)$: SSA: AAE	-0.22±0.11	-0.36±0.10	-0.49±0.11
	*	***	***
*** p < 0.001; ** p < 0.01; * p < 0.05; . p < 0.1.			

- *Assessment of the fit of regression models*

After selecting the model, we performed “F-test” to determine whether the model with fewer variables predicted $\frac{B_{abs}}{B_{ATN}}$ better than the model with all predictors. The F-tests indicated that dropping any predictor did not improve the fit of the model (F-ratios $\gg 1$ and P-value < 0.05).

We then analyzed the residuals of the selected model to test the adequacy of prediction. We found that the residuals were well scattered in a random pattern against $\ln(\text{Tr})$, SSA and AAE (Fig. S2), indicating that the models as presented in Eq. (10) in the main text give the best accuracy.

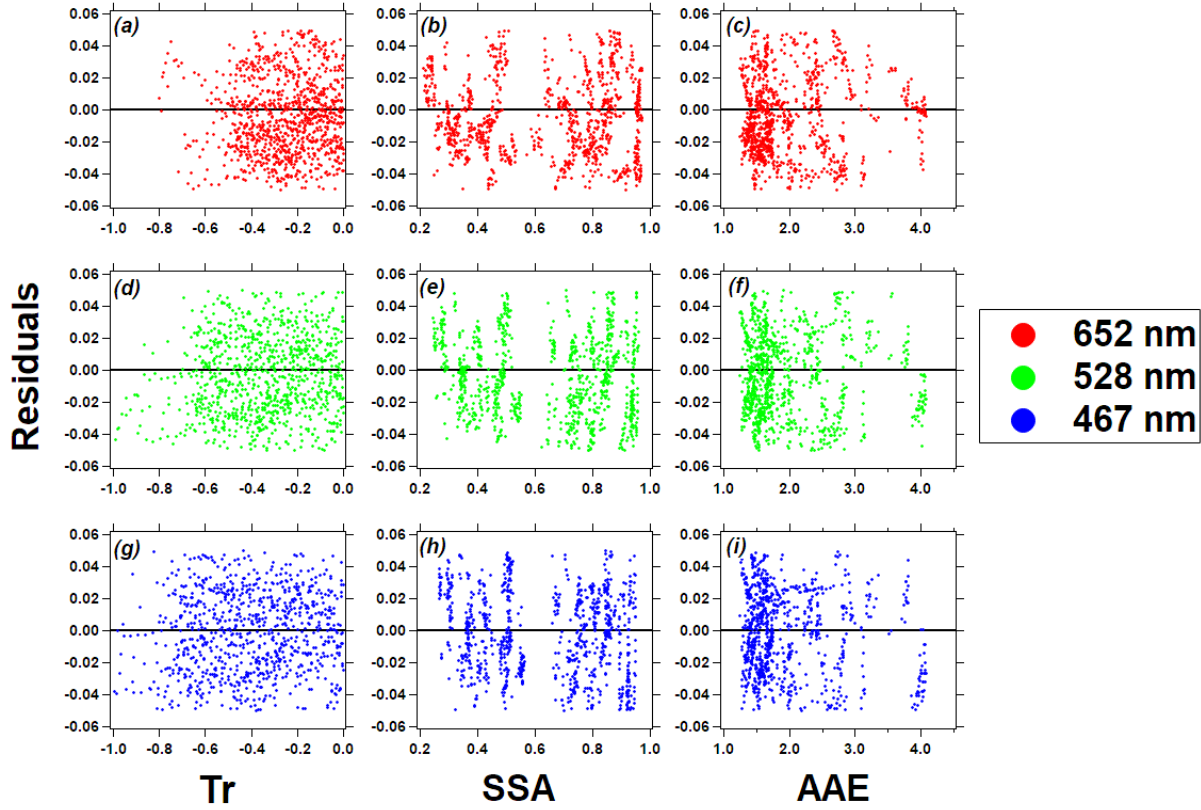


Figure S2. Scatter plot of residuals against Tr, SSA, and AAE at 652 nm, 528 nm, and 467 nm.

The above analyses were then repeated for TAP-related observations. The results were consistent with what we have found on the CLAP data. We present the final regression models to predict $\frac{B_{\text{abs}}}{B_{\text{ATN}}}$ for these TAP-related observations in Table S4.

Table S4 Predictors of $\frac{B_{abs}}{B_{ATN}}$ for TAP-related observations

	652 nm	528 nm	467 nm
R ²	0.36	0.32	0.35
Intercept	0.03±0.11	0.02±0.12	0.16±0.11
ln(Tr)	-1.20±0.39 **	-0.97±0.33 **	-0.53±0.28 *
SSA	0.48±0.11 ***	0.40±0.12 ***	0.25±0.12 *
AAE	0.20±0.07 **	0.18±0.08 *	0.10±0.08
ln(Tr): SSA	1.43±0.41 ***	0.99±0.34 **	0.49±0.29 .
SSA: AAE	-0.28±0.08 ***	-0.23±0.08 **	-0.15±0.08 .
ln(Tr): AAE	0.55±0.26 *	0.44±0.23 *	0.18±0.13
ln(Tr): SSA: AAE	-0.62±0.28 *	-0.47±0.24 *	-0.20±0.20
*** p < 0.001; ** p < 0.01; * p < 0.05; . p < 0.1.			

- *Interpretation of the regression models*

We can order the terms in Eq. (10) into two groups, the first group (terms that do not contain ln(Tr): $(G_0 + G_2 \times SSA(\lambda) + G_3 \times AAE + G_6 \times SSA(\lambda) \times AAE)$) defines the intercept on a graph of $\frac{B_{abs}}{B_{ATN}}$ against ln(Tr); the second group (all terms that contain the ln(Tr): $\ln(Tr)(\lambda) \times (G_1 + G_4 \times SSA(\lambda) + G_5 \times AAE + G_7 \times SSA(\lambda) \times AAE)$) defines the simple slope of the line (Dawson and Richter, 2006; Zedeck, 1971). As in this form, the new correction equation can be interpreted as following:

1. For a given wavelength, the relation between ln(Tr) and $\frac{B_{abs}}{B_{ATN}}$ varies across levels of SSA and AAE, and the combination of SSA and AAE.
2. Under different conditions of SSA and AAE, the same value of ln(Tr) may lead to various ratios between B_{abs} and B_{ATN} , and the compensation and/or reduction of B_{ATN} will be different to agree with the reference B_{abs} .

We also conduct simple slope analyses to explore the nature of the three-way interaction terms (Aiken et al., 1991). Specifically, we arbitrary assume four combinations of AAE and SSA: (1). SSA=0.95 and AAE=4; (2). SSA=0.8 and AAE=3; (3). SSA=0.8 and AAE=1.5; (4). SSA=0.4 and AAE=1. As seen in Fig. S3 (528 nm as an example), the $\frac{B_{abs}}{B_{ATN}}$ -ln(Tr) relationship is moderated by different combinations of AAE and SSA. For example, the slope of “Comb. 4” in Fig. S3(b) is significantly different ($p < 0.05$) from the slopes of other three combinations of SSA and AAE. Moreover, the intercept of the four lines are inconsistent, indicating that even when the filter is slightly loaded ($\ln(Tr) \rightarrow 0$), the correction of B_{ATN} should be different for the aerosols with various optical properties.

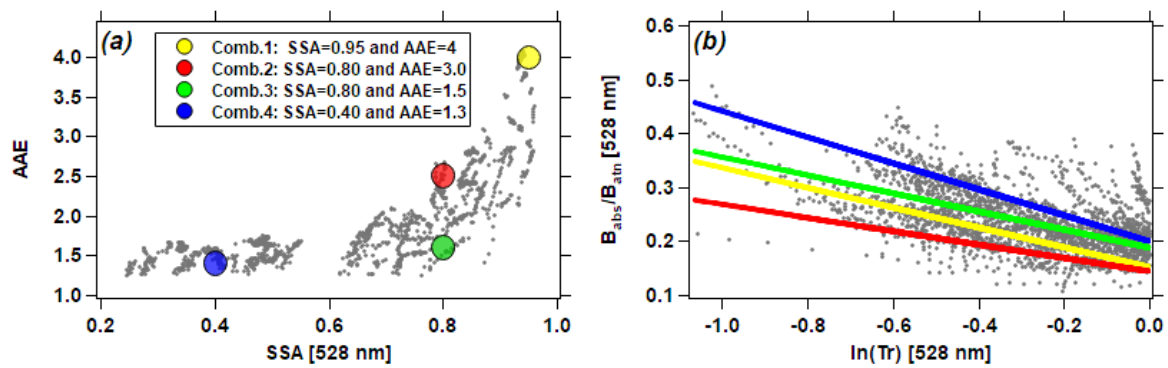


Figure S3. Simple slopes analysis of cross-level interaction of SSA and AAE in predicting $\frac{B_{\text{abs}}}{B_{\text{ATN}}}$ as a function of $\ln(\text{Tr})$ at 528 nm.

2. The procedure for simulating the uncertainty of the new algorithms in Section 3.5

The simulation is performed in seven steps:

1. We arbitrarily set concentration ranges of “true” B_{abs} at 652 nm from 100 to 2500 Mm^{-1} and AAE from 0.5 to 4.5 (number of cases = 500).
2. For each combination of “true” B_{abs} at 652 nm and AAE (500×500 in total), we calculate the B_{abs} at 528 and 467 nm. For example, $B_{\text{abs}}(467 \text{ nm}) = B_{\text{abs}}(652 \text{ nm}) \times (467/652)^{-\text{AAE}}$.
3. With the observed power relationship between AAE and SSA (similar to Fig. 6 in the main text, but using B_{abs} instead of B_{ATN} as the absorption measurements), we compute SSA for each AAE value. The derived SSA is then used to calculate B_{scat} ($B_{\text{scat}} = \text{SSA}/(1-\text{SSA}) \times B_{\text{abs}}$).
4. With the observed relationship between B_{abs} and B_{ATN} (Fig. 3 in the main text), we calculate the filter-based B_{ATN} at all three wavelengths.
5. We simulate the measurements of filter-based B_{ATN} , photoacoustic B_{abs} , and NEPH-derived B_{scat} by adding the measurement uncertainty of the instruments to the parameters described in Steps 1-4. The measurement uncertainties are forms of normal distribution (Table 1 in the main text). Figure S4 shows an example of a dataset derived by Steps 1-5.
6. We implement “Algorithm B” on the derived dataset from Step 5. The corrected filter-based results are then compared to the “true” B_{abs} .
7. The above procedure is repeated 1000 times using a Monte Carlo simulation to evaluate bias and power of our correction algorithms.

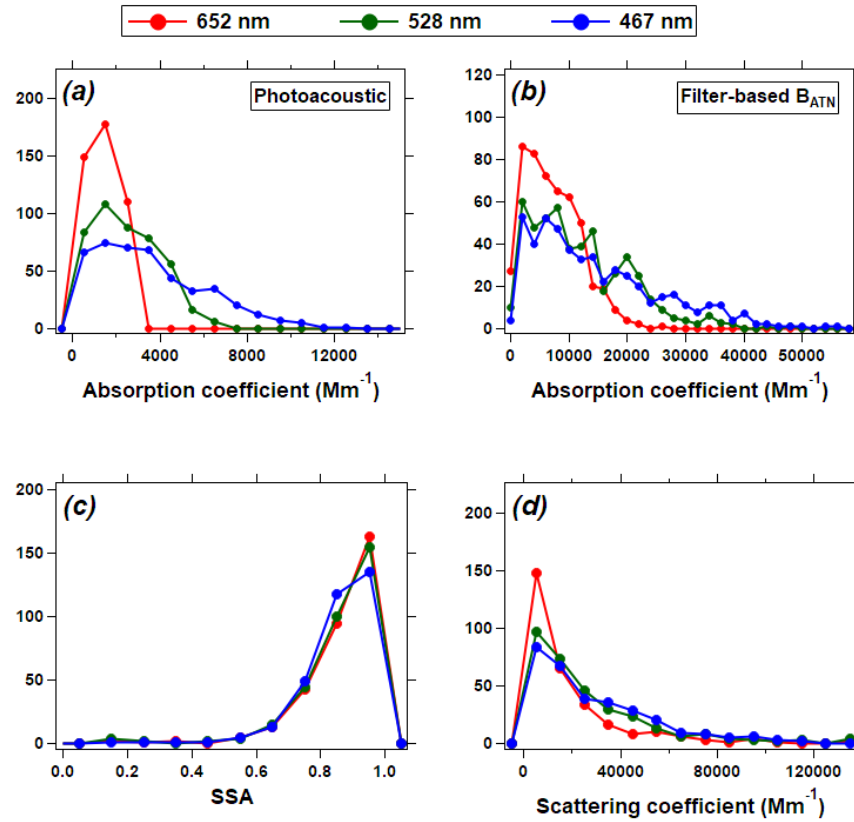


Figure S4. Distribution of the simulated measurements derived by Steps 1-5 in the above procedure.

SUPPLEMENTARY TABLES

Table S5 Relationship between the filter-based B_{abs} (FIREX-TAP and SGP-PSAP) corrected by B1999 and V2005 algorithms and the reference B_{abs} at 652, 528, and 467 nm. This table complements Table 3 from in the main text.

		652 nm	528 nm	467 nm
FIREX -TAP	B1999	$y = -46 + 2.17x$ (0.83)	$y = -55 + 1.88x$ (0.85)	$y = -61 + 1.75x$ (0.86)
	V2005	$y = -50 + 2.23x$ (0.85)	$y = -62 + 2.03x$ (0.85)	$y = -76 + 2.07x$ (0.86)
	B1999 (update coeffs)	$y = -12 + 1.00x$ (0.85)	$y = -17 + 1.00x$ (0.86)	$y = -19 + 0.99x$ (0.87)
	V2005 (update coeffs)	$y = -13 + 1.02x$ (0.87)	$y = -16 + 1.00x$ (0.87)	$y = -16 + 0.99x$ (0.87)
SGP -PSAP	B1999	$y = -6.40 + 5.86x$ (0.32)	$y = -5.24 + 4.47(0.43)$	$y = -4.10 + 3.88x$ (0.51)
	V2005	$y = -7.10 + 6.10x$ (0.32)	$y = -6.72 + 5.11x$ (0.40)	$y = -5.43 + 5.43x$ (0.49)
	B1999 (update coeffs)	$y = -0.52 + 1.21x$ (0.40)	$y = -0.57 + 1.18x$ (0.50)	$y = -0.37 + 1.09x$ (0.55)
	V2005 (update coeffs)	$y = -0.89 + 1.40x$ (0.46)	$y = -0.76 + 1.24x$ (0.52)	$y = -0.45 + 1.11x$ (0.58)

Table S6 Inter-comparison between different filter-based B_{abs} corrected by the same algorithm. The value in the bracket represents the coefficient of determination (R^2) of the linear relationship.

		FIREX: CLAP vs. TAP	SGP: CLAP vs. PSAP
B1999	652 nm	$y = 7.00 + 1.29x$ (0.91)	$y = 0.61 + 0.77x$ (0.57)
	528 nm	$y = 13.61 + 1.36x$ (0.90)	$y = 1.09 + 0.78x$ (0.53)
	467 nm	$y = 25.40 + 1.30x$ (0.89)	$y = 1.61 + 0.75x$ (0.55)
V2005	652 nm	$y = 4.42 + 1.33x$ (0.90)	$y = 0.87 + 0.68x$ (0.54)
	528 nm	$y = 12.07 + 1.40x$ (0.89)	$y = 1.39 + 0.69x$ (0.53)
	467 nm	$y = 28.84 + 1.32x$ (0.88)	$y = 1.85 + 0.68x$ (0.56)
B1999 (update coeffs)	652 nm	$y = 4.20 + 1.01x$ (0.88)	$y = 0.01 + 0.96x$ (0.61)
	528 nm	$y = 8.02 + 1.01x$ (0.86)	$y = 0.16 + 0.91x$ (0.65)
	467 nm	$y = 13.18 + 1.01x$ (0.85)	$y = 0.21 + 0.90x$ (0.70)
V2005 (update coeffs)	652 nm	$y = 3.30 + 1.02x$ (0.89)	$y = 0.08 + 0.92x$ (0.68)
	528 nm	$y = 6.81 + 1.01x$ (0.87)	$y = 0.18 + 0.90x$ (0.68)
	467 nm	$y = 11.00 + 1.01x$ (0.85)	$y = 0.24 + 0.90x$ (0.72)

Table S7 Updated coefficients in the B1999 and V2005 algorithms using our data ^a.

				C2	C3	C1		
B1999 ^b	FIREX	CLAP	652 nm	3.42	2.00	0.016		
			528 nm	3.47	1.77	0.016		
			467 nm	3.49	1.43	0.016		
		TAP	652 nm	1.58	2.13	0.016		
			528 nm	1.19	2.07	0.016		
			467 nm	1.11	1.93	0.016		
	SGP	CLAP	652 nm	-1.39	6.12	0.016		
			528 nm	0.88	4.03	0.016		
			467 nm	1.51	3.46	0.016		
		PSAP	652 nm	1.730	3.930	0.016		
			528 nm	2.230	3.180	0.016		
			467 nm	2.590	2.940	0.016		
				C4	C5	C6	C7	C1
V2005 ^c	FIREX	CLAP	652 nm	0.19	-0.34	0.90	-0.83	0.022
			528 nm	0.19	-0.23	0.95	-0.50	0.017
			467 nm	0.20	-0.19	0.95	-0.15	0.015
		TAP	652 nm	0.28	-0.44	0.88	-1.07	0.022
			528 nm	0.31	-0.36	0.94	-0.94	0.017
			467 nm	0.32	-0.35	0.92	-0.79	0.015
	SGP	CLAP	652 nm	0.22	-1.22	1.14	-1.22	0.022
			528 nm	0.20	-0.94	1.07	-1.09	0.017
			467 nm	0.20	-0.78	1.01	-0.99	0.015
		PSAP	652 nm	0.19	-0.55	0.98	-0.92	0.022
			528 nm	0.19	-0.48	1.00	-0.90	0.017
			467 nm	0.18	-0.44	0.96	-0.84	0.015

^a We update the coefficients in B1999 and V2005 using the Levenberg-Marquardt algorithm (Levenberg, 1944), which is different from the original approach to fitting the coefficients in those papers. Specifically, we hold C₁ to be the same as the value in B1999 and V2005 and iteratively fit the other coefficients until the chi-square of the coefficients are minimized.

^b The general form of the B1999 algorithm: $B_{\text{abs}} = B_{\text{ATN}} \times \frac{1}{C_2 \times \text{Tr} + C_3} - C_1 \times B_{\text{scat}}$

^c The general form of the V2005 algorithm: $B_{\text{abs}} = B_{\text{ATN}} \times C_4 + C_5 \times (C_6 + C_7 \times \text{SSA}) \times \ln(\text{Tr}) - C_1 \times B_{\text{scat}}$

Table S8 Updated coefficients in the B1999 algorithm using different subsets of AAE and SSA for the FIREX measurements. The aerosols with different subranges of AAE and SSA result in different values of C2 and C3 for different wavelengths, which are different from the “default” values in B1999. The blank cells represent combinations with no available data.

CLAP	C2		wavelength	SSA			TAP	C2		wavelength	SSA		
				<0.4	0.4-0.8	0.8-1					<0.4	0.4-0.8	0.8-1
	AAE	<1.8	652 nm	4.384	3.249			AAE	<1.8	652 nm	3.419	1.917	
			528 nm	3.988	3.395					528 nm	3.196	1.929	
			467 nm	3.778	3.132					467 nm	2.954	1.895	
		1.8-3.4	652 nm		3.312	1.583			1.8-3.4	652 nm		1.355	-3.209
			528 nm		4.150	2.656				528 nm		2.462	-1.184
			467 nm		3.982	2.576				467 nm		2.761	-0.330
	>3.4	652 nm		3.908	>3.4	652 nm			0.992				
		528 nm		3.800		528 nm			1.212				
467 nm		3.619		467 nm		1.537							
C3		wavelength	SSA			C3		wavelength	SSA				
			<0.4	0.4-0.8	0.8-1				<0.4	0.4-0.8	0.8-1		
AAE	<1.8	652 nm	0.623	2.049		AAE	<1.8	652 nm	0.101	2.098			
		528 nm	0.960	1.664				528 nm	0.234	1.563			
		467 nm	0.941	1.619				467 nm	0.380	1.394			
	1.8-3.4	652 nm		2.726	4.085		1.8-3.4	652 nm		2.664	6.215		
		528 nm		1.768	2.618			528 nm		1.228	3.791		
		467 nm		1.733	2.143			467 nm		0.549	2.930		
	>3.4	652 nm		1.881	>3.4		652 nm		3.503				
		528 nm		1.199			528 nm		2.365				
		467 nm		0.872			467 nm		1.835				

Table S9 Updated coefficients in the V2005 algorithm using different subsets of AAE and SSA for the FIREX measurements. The aerosols with different subranges of AAE and SSA result in different values of C4 - C7 for different wavelengths, which are different from the “default” values in V2005. The blank cells represent combinations with no available data.

CLAP	C4		wavelength	SSA		
				<0.4	0.4-0.8	0.8-1
	AAE	<1.8	652 nm	0.194	0.189	
			528 nm	0.197	0.189	
			467 nm	0.204	0.200	
		1.8-3.4	652 nm		0.169	0.184
			528 nm		0.172	0.192
			467 nm		0.173	0.210
		>3.4	652 nm			0.191
			528 nm			0.202
467 nm					0.218	
C5		wavelength	SSA			
			<0.4	0.4-0.8	0.8-1	
AAE	<1.8	652 nm	-0.353	-0.225		
		528 nm	-0.384	-0.318		
		467 nm	-0.362	-0.343		
	1.8-3.4	652 nm		-0.070	-0.035	
		528 nm		0.188	-0.059	
		467 nm		-0.093	-0.489	
	>3.4	652 nm			-0.277	
		528 nm			-0.392	
		467 nm			-0.216	
C6		wavelength	SSA			
			<0.4	0.4-0.8	0.8-1	
AAE	<1.8	652 nm	0.795	0.852		
		528 nm	0.861	0.880		
		467 nm	0.814	0.851		
	1.8-3.4	652 nm		1.026	1.038	
		528 nm		2.230	-0.327	
		467 nm		-2.056	0.979	
	>3.4	652 nm			1.071	
		528 nm			1.094	
		467 nm			0.969	
C7		wavelength	SSA			
			<0.4	0.4-0.8	0.8-1	
AAE	<1.8	652 nm	-0.517	-0.579		
		528 nm	-1.016	-0.810		
		467 nm	-0.645	-0.784		
	1.8-3.4	652 nm		0.341	0.209	
		528 nm		-3.842	2.175	
		467 nm		4.561	-0.863	
	>3.4	652 nm			-0.631	
		528 nm			-0.691	
		467 nm			0.044	

TAP	C4		wavelength	SSA		
				<0.4	0.4-0.8	0.8-1
	AAE	<1.8	652 nm	0.276	0.254	
			528 nm	0.280	0.284	
			467 nm	0.285	0.302	
		1.8-3.4	652 nm		0.254	0.335
			528 nm		0.280	0.376
			467 nm		0.291	0.379
		>3.4	652 nm			0.245
			528 nm			0.285
467 nm					0.297	
C5		wavelength	SSA			
			<0.4	0.4-0.8	0.8-1	
AAE	<1.8	652 nm	-0.057	-0.075		
		528 nm	-0.175	-0.365		
		467 nm	-0.146	-0.507		
	1.8-3.4	652 nm		-2.349	-1.234	
		528 nm		-4.758	-0.740	
		467 nm		-1.298	0.224	
	>3.4	652 nm			0.202	
		528 nm			-0.093	
		467 nm			-0.216	
C6		wavelength	SSA			
			<0.4	0.4-0.8	0.8-1	
AAE	<1.8	652 nm	-6.739	0.613		
		528 nm	-0.605	0.945		
		467 nm	-1.151	0.933		
	1.8-3.4	652 nm		1.141	1.130	
		528 nm		0.976	0.938	
		467 nm		1.115	0.900	
	>3.4	652 nm			0.750	
		528 nm			1.106	
		467 nm			1.004	
C7		wavelength	SSA			
			<0.4	0.4-0.8	0.8-1	
AAE	<1.8	652 nm	41.858	0.725		
		528 nm	8.037	-0.892		
		467 nm	10.428	-1.052		
	1.8-3.4	652 nm		-1.472	-1.474	
		528 nm		-1.240	-1.238	
		467 nm		-1.133	-0.904	
	>3.4	652 nm			-1.031	
		528 nm			-0.248	
		467 nm			-0.487	

Table S10 Updated coefficients in the B1999 algorithm using different subsets of AAE and SSA for the SGP measurements. The aerosols with different subranges of AAE and SSA result in different values of C2 and C3 for different wavelengths, which are different from the “default” values in B1999. The blank cells represent combinations with no available data.

CLAP	C2		wavelength	SSA		
	AAE	<1	652 nm	1.045	-1.532	3.071
			528 nm	1.894	1.559	2.141
			467 nm	1.362	4.005	2.165
		1-2	652 nm		0.110	-7.351
			528 nm		1.966	-1.961
			467 nm		2.069	0.175
		>2	652 nm			-0.276
			528 nm			3.928
			467 nm			2.900
C3	wavelength	SSA				
AAE	<1	652 nm	3.684	6.600	3.825	
		528 nm	3.165	4.198	4.612	
		467 nm	3.751	2.258	4.735	
	1-2	652 nm		5.480	12.699	
		528 nm		3.667	7.489	
		467 nm		3.592	5.476	
	>2	652 nm			6.255	
		528 nm			1.805	
		467 nm			2.551	

PSAP	C2		wavelength	SSA		
	AAE	<1	652 nm	3.887	-0.461	1.924
			528 nm	4.164	-1.480	3.588
			467 nm	4.627	0.858	1.154
		1-2	652 nm		1.186	1.376
			528 nm		2.555	2.338
			467 nm		3.234	2.719
		>2	652 nm			1.959
			528 nm			1.989
			467 nm			2.551
C3	wavelength	SSA				
AAE	<1	652 nm	2.308	6.071	4.609	
		528 nm	2.072	6.907	3.571	
		467 nm	2.081	5.358	5.217	
	1-2	652 nm		4.761	5.033	
		528 nm		3.367	3.849	
		467 nm		3.031	3.515	
	>2	652 nm			4.939	
		528 nm			3.747	
		467 nm			3.212	

Table S11 Updated coefficients in the V2005 algorithm using different subsets of AAE and SSA for the SGP measurements. The aerosols with different subranges of AAE and SSA result in different values of C4 - C7 for different wavelengths, which are different from the “default” values in V2005. The blank cells represent combinations with no available data.

CLAP	C4		wavelength	SSA		
				<0.8	0.8-0.9	0.9-1
			652 nm	0.210	0.202	0.152
	AAE	<1	528 nm	0.196	0.172	0.152
			467 nm	0.193	0.159	0.145
			652 nm		0.184	0.194
		1-2	528 nm		0.179	0.182
			467 nm		0.176	0.176
			652 nm			0.172
		>2	528 nm			0.176
			467 nm			0.182
		C5		wavelength	SSA	
				<0.8	0.8-0.9	0.9-1
	AAE	<1	652 nm	-0.596	-2.474	-2.370
			528 nm	-0.517	-1.512	-1.681
			467 nm	-0.571	-1.161	-1.102
		1-2	652 nm		-1.378	-3.306
			528 nm		-0.267	-1.799
			467 nm		-0.182	-1.509
		>2	652 nm			-2.253
			528 nm			1.733
			467 nm			-0.094
	C6		wavelength	SSA		
				<0.8	0.8-0.9	0.9-1
	AAE	<1	652 nm	0.922	1.027	1.204
			528 nm	0.943	1.403	1.242
			467 nm	0.922	1.125	0.998
		1-2	652 nm		1.183	1.276
			528 nm		0.965	1.215
			467 nm		0.952	1.104
		>2	652 nm			1.415
			528 nm			1.162
			467 nm			0.957
	C7		wavelength	SSA		
				<0.8	0.8-0.9	0.9-1
	AAE	<1	652 nm	-1.124	-1.216	-1.256
			528 nm	-1.084	-1.579	-1.313
			467 nm	-1.111	-1.194	-1.036
		1-2	652 nm		-1.371	-1.426
528 nm				-0.862	-1.336	
467 nm				-0.718	-1.187	
>2		652 nm			-1.500	
		528 nm			-1.335	
		467 nm			0.065	

PSAP	C4		wavelength	SSA		
				<0.8	0.8-0.9	0.9-1
			652 nm	0.172	0.182	0.163
	AAE	<1	528 nm	0.161	0.183	0.146
			467 nm	0.144	0.159	0.154
			652 nm		0.171	0.167
		1-2	528 nm		0.170	0.166
			467 nm		0.159	0.163
			652 nm			0.157
		>2	528 nm			0.178
			467 nm			0.174
		C5		wavelength	SSA	
				<0.8	0.8-0.9	0.9-1
	AAE	<1	652 nm	-0.805	0.611	-0.137
			528 nm	-0.624	0.133	-0.072
			467 nm	-0.986	-0.535	-0.049
		1-2	652 nm		-0.652	-0.008
			528 nm		-0.411	-0.084
			467 nm		-0.381	-0.032
		>2	652 nm			0.773
			528 nm			-0.094
			467 nm			-0.058
	C6		wavelength	SSA		
				<0.8	0.8-0.9	0.9-1
	AAE	<1	652 nm	1.024	0.865	0.977
			528 nm	1.002	0.569	1.116
			467 nm	1.036	0.921	0.870
		1-2	652 nm		0.949	1.289
			528 nm		0.973	1.025
			467 nm		0.937	0.976
		>2	652 nm			0.854
			528 nm			1.043
			467 nm			1.053
	C7		wavelength	SSA		
				<0.8	0.8-0.9	0.9-1
	AAE	<1	652 nm	-1.269	-0.994	-0.739
			528 nm	-1.096	-0.412	-0.317
			467 nm	-1.190	-1.019	-0.410
		1-2	652 nm		-1.025	2.107
528 nm				-0.922	-0.477	
467 nm				-0.837	2.856	
>2		652 nm			-0.961	
		528 nm			-0.548	
		467 nm			0.088	

Table S12 Computation of the quartile deviation for the derived coefficient values in “Algorithm A” using half of the CLAP observation. The box-and-whisker plots of the derived coefficient values are presented in Fig. S7.

	FIREX			SGP		
	652 nm	528 nm	467 nm	652 nm	528 nm	467 nm
G0	0.012	0.012	0.015	0.043	0.037	0.043
G1	0.057	0.047	0.049	0.428	0.333	0.309
G2	0.023	0.022	0.025	0.059	0.050	0.056
G3	0.008	0.009	0.010	0.035	0.029	0.032
G4	0.094	0.077	0.074	0.573	0.409	0.388
G5	0.013	0.013	0.015	0.050	0.041	0.042
G6	0.044	0.036	0.035	0.340	0.244	0.224
G7	0.068	0.036	0.054	0.460	0.334	0.285

SUPPLEMENTARY FIGURES

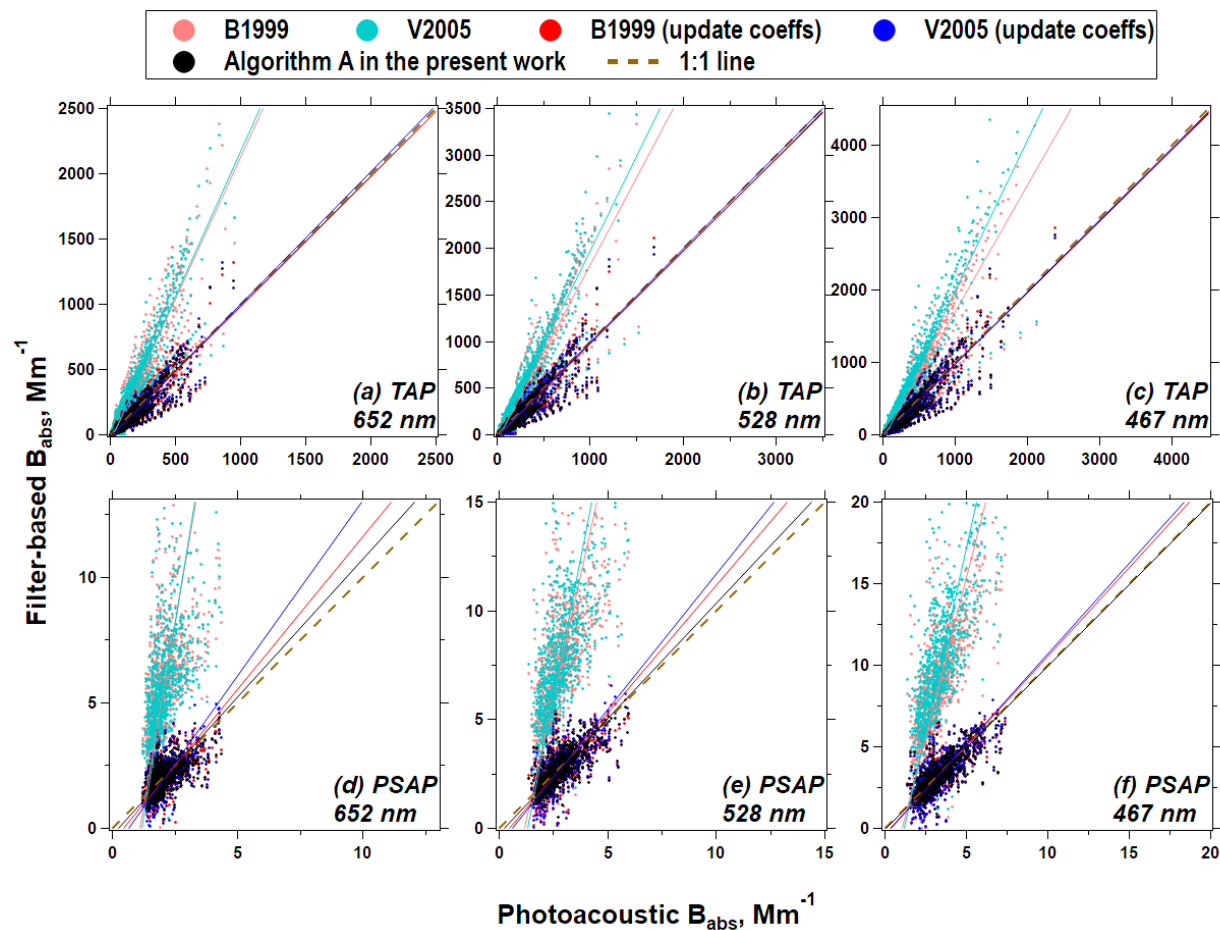


Figure S5. Inter-comparison between the filter-based B_{abs} (FIREX-TAP and SGP-PSAP) corrected by different algorithms and the reference B_{abs} at 652, 528, and 467 nm. The solid lines represent linear regressions, while the dashed line is a 1:1 line.

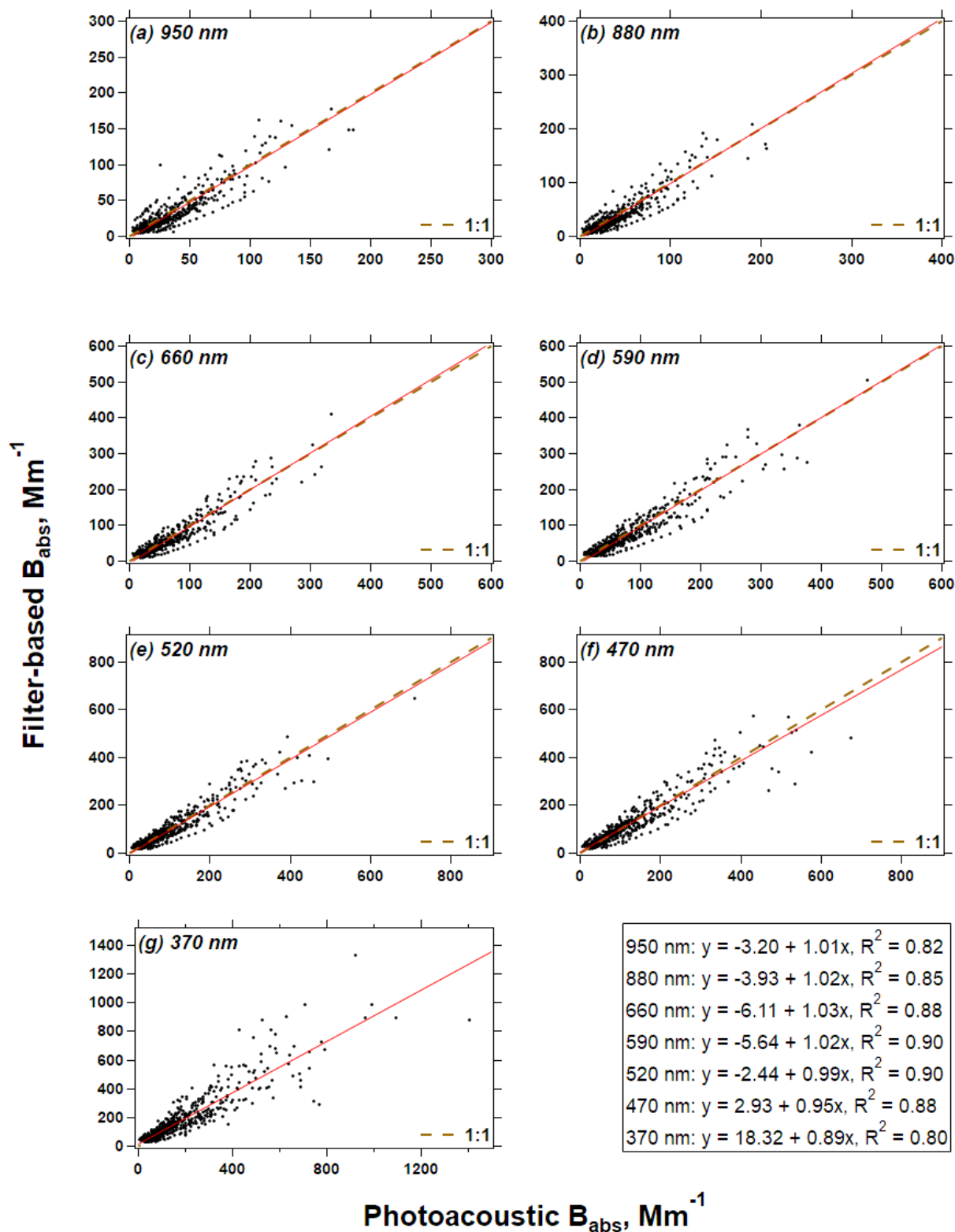
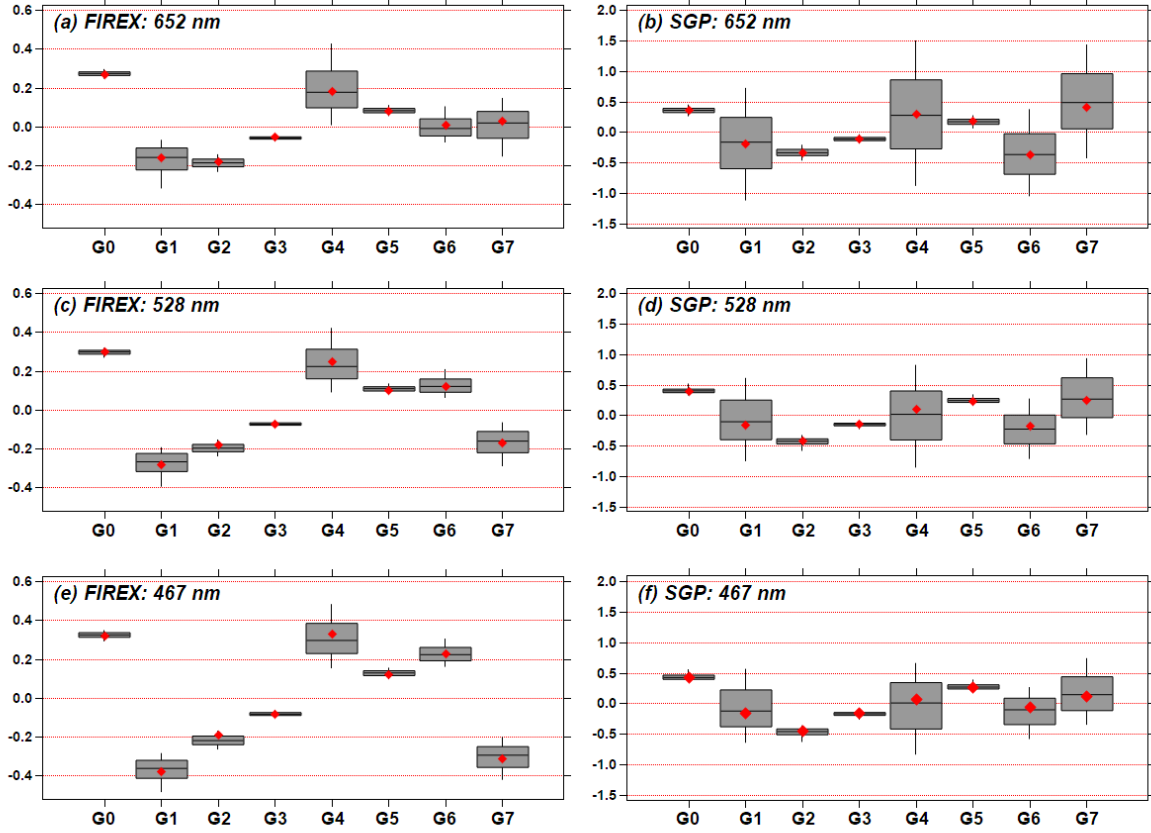


Figure S6. The AETH-derived B_{abs} (corrected by “Algorithm A” in the present work) versus photoacoustic B_{abs} for the FIREX aerosols. The solid lines represent a linear regression, while the dashed lines are 1:1 lines.



Derived coefficient values using “Algorithm A”

Figure S7. The distribution of derived coefficient values for “Algorithm A” using half of the CLAP observation. The red dots represent the coefficient values derived using all observations (as shown in Table 4).

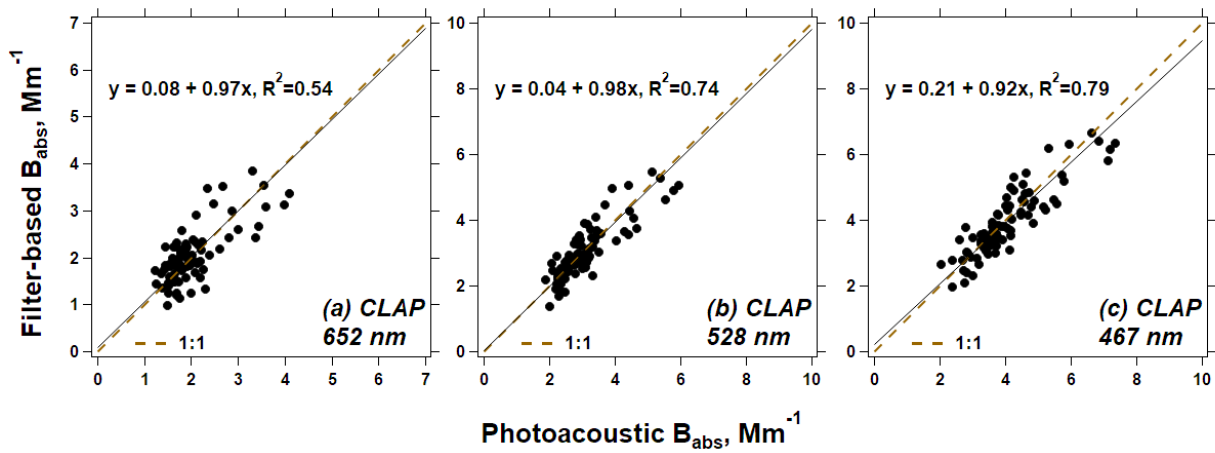


Figure S8. Inter-comparison between the CLAP-derived B_{abs} corrected by “Algorithm C” in the present work and reference B_{abs} at 652, 528, and 467 nm for the subsamples of SGP measurements (AAE-SSA prediction error is within 30%). The solid lines represent a linear regression, while the dashed lines are 1:1 lines.

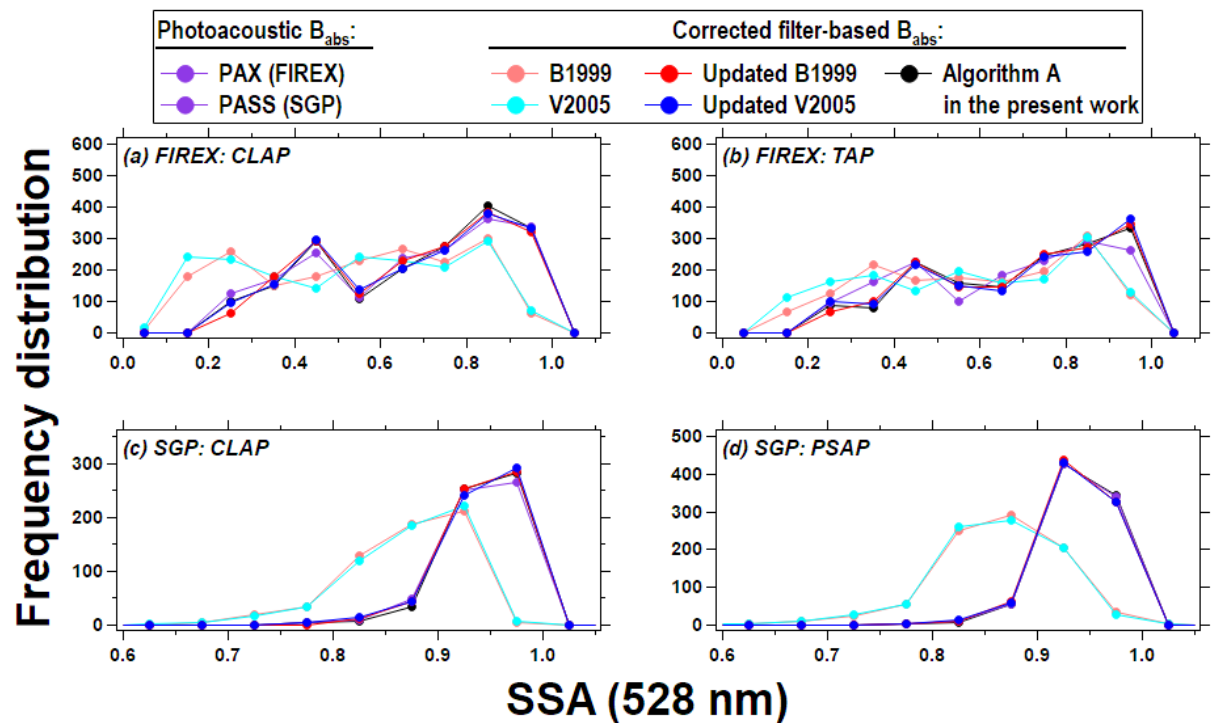


Figure S9. The frequency distribution of SSA (528 nm) calculated for different instrument/correction combinations of B_{abs} and B_{scat} .

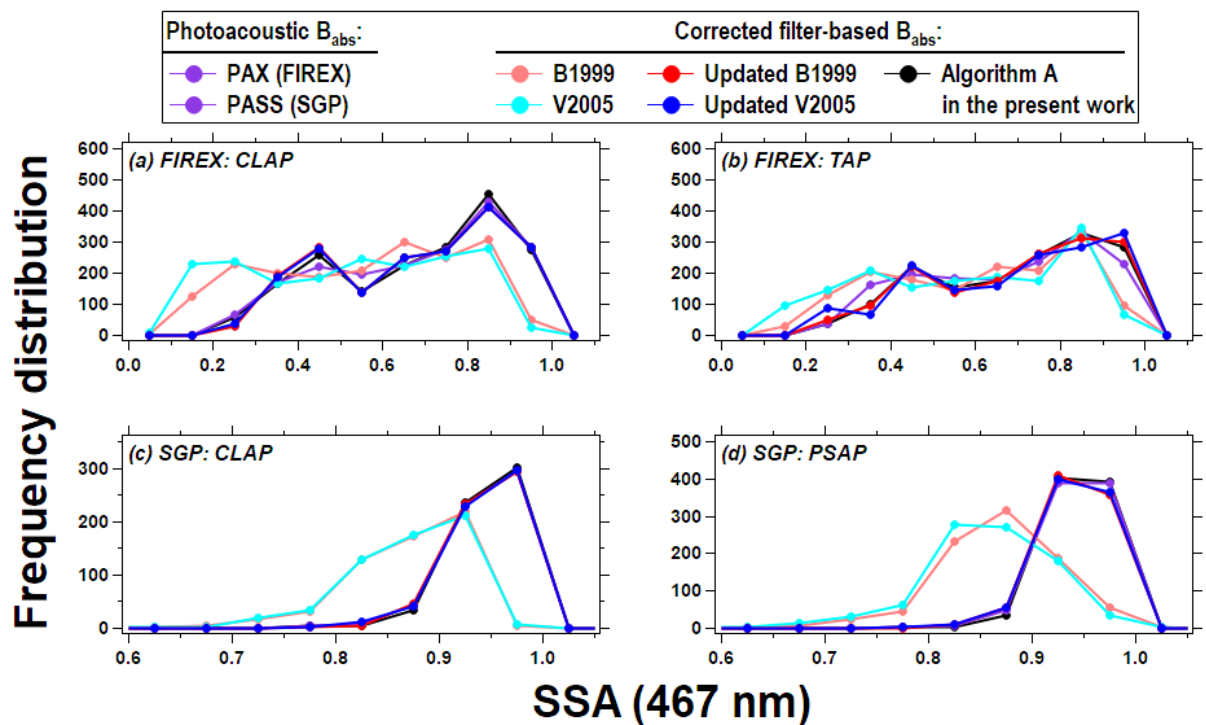


Figure S10. The frequency distribution of SSA (467 nm) calculated for different instrument/correction combinations of B_{abs} and B_{scat} .

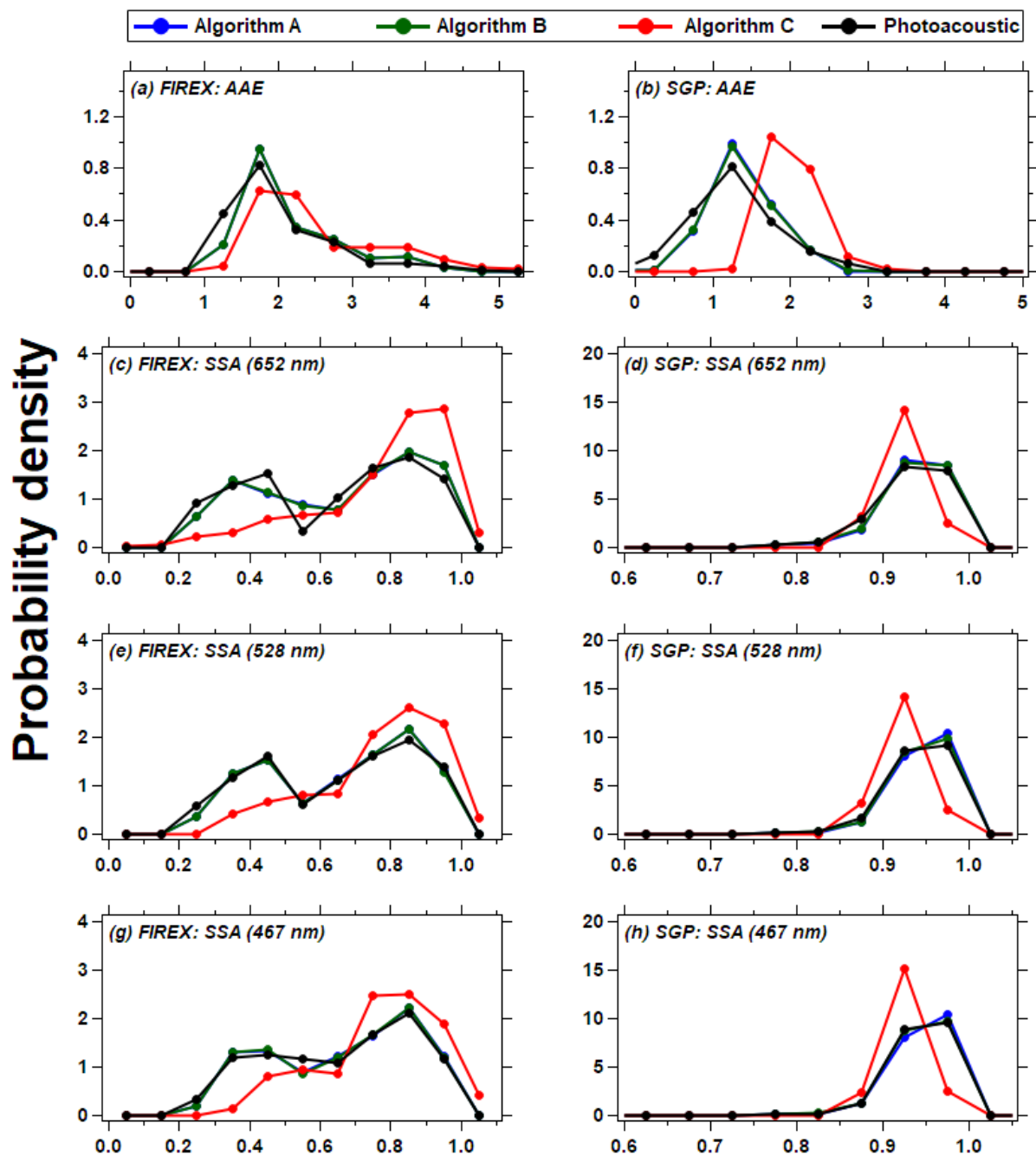


Figure S11. The probability density of AAE and SSA computed by the new algorithms (A, B, C) for the FIREX and SGP CLAP data. The curves of “Algorithm A” and “Algorithm B” overlap in some panels.

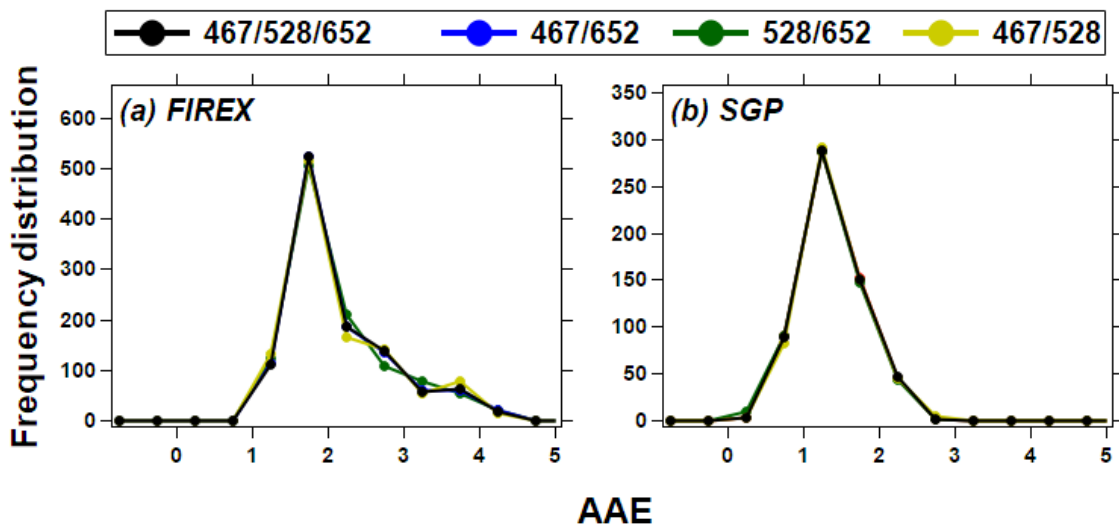


Figure S12. The frequency distribution of AAE calculated by different wavelength combinations (derived by “Algorithm A” in the present work).

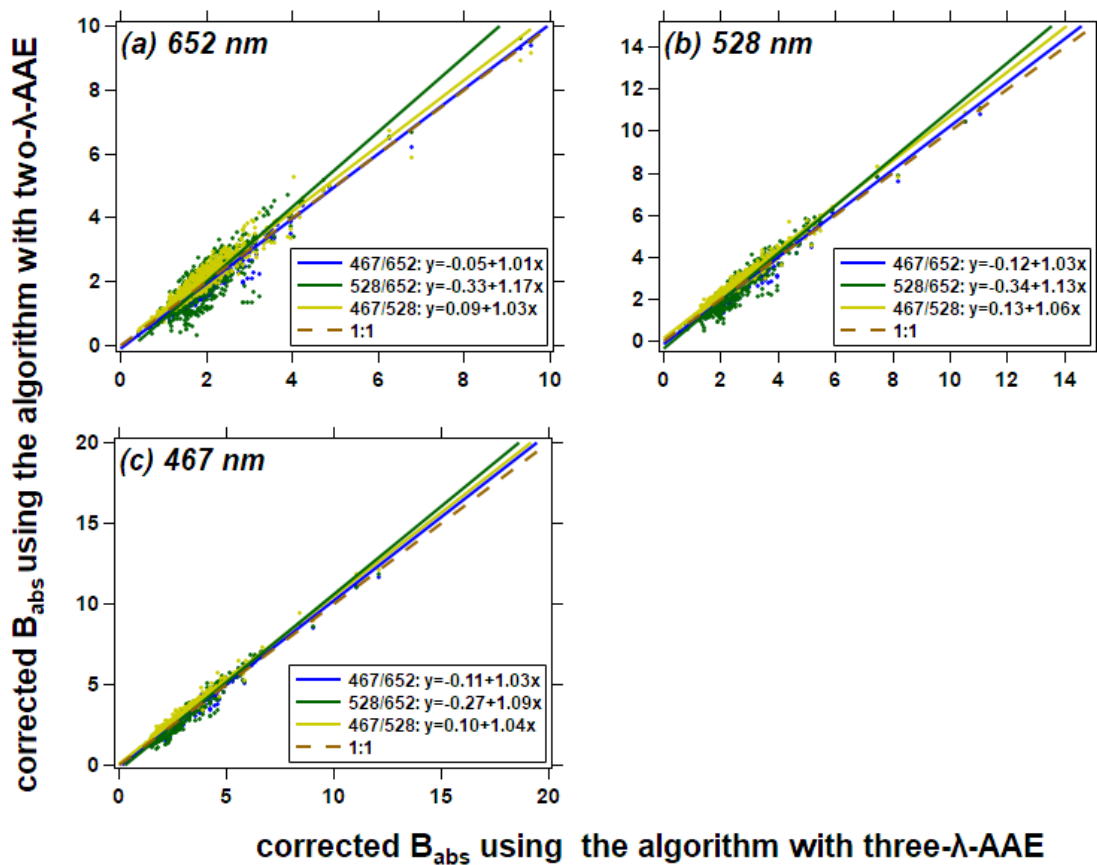


Figure S13. Inter-comparison of SGP-CLAP- B_{abs} derived by “Algorithm A” with different calculation of AAE.

REFERENCES

- Aiken, L.S., West, S.G., Reno, R.R., 1991. Multiple regression: Testing and interpreting interactions. Sage.
- Benoit, K., 2011. Linear regression models with logarithmic transformations. *London Sch. Econ. London* 22, 23–36.
- Creamer, D.B., Henyey, F., Schult, R., Wright, J., 1989. Improved linear representation of ocean surface waves. *J. Fluid Mech.* 205, 135–161.
- Dawson, J.F., Richter, A.W., 2006. Probing three-way interactions in moderated multiple regression: Development and application of a slope difference test. *J. Appl. Psychol.* 91, 917–926. <https://doi.org/10.1037/0021-9010.91.4.917>
- Lek, S., Delacoste, M., Baran, P., Dimopoulos, I., Lauga, J., Aulagnier, S., 1996. Application of neural networks to modelling nonlinear relationships in ecology. *Ecol. Modell.* 90, 39–52.
- Levenberg, K., 1944. A method for the solution of certain non-linear problems in least squares. *Q. Appl. Math.* 2, 164–168.
- Zedeck, S., 1971. Problems with the use of “moderator” variables. *Psychol. Bull.* 76, 295–310. <https://doi.org/10.1037/h0031543>